Supporting Information for "Ultra-dense, deep sub-wavelength nanowire array photovoltaics as engineered optical thin films"

Ion implantation

The silicon-on-insulator (SOI) substrates (Soitec USA Inc., Peabody, MA) were implanted with dopant ions (CORE Systems, Sunnyvale, CA) through photoresist masks. Heavily-doped *p*-type (dose of 3.8×10^{14} cm^{-2} B^+ at 2.5 keV) and *n*-type (dose of 3.2×10^{14} cm^{-2} P^+ at 6.5 keV) contact regions were used to promote the formation of ohmic contacts, while the device regions received a low- or high-dose *p*-type implant (dose of 3.8×10^{10} cm^{-2} B^+ or 3.8×10^{13} cm^{-2} B^+ at 2.5 keV). All implants were performed at an off-normal angle of 7° to mitigate implant profile broadening due to ion channeling.

Modified RCA clean

Our modified RCA cleaning recipe consists of a three-step procedure in solutions of H_2SO_4:H_2O_2 (3:1 v/v, 90 °C, 10 min), HF:H_2O (1:50 v/v, 15 s in dark), and H_2O:HCl:H_2O_2 (6:1:1, 80 °C, 10 min). After each step, the substrate was rinsed thoroughly with de-ionized water and dried with dry N_2.

Superlattice nanowire pattern transfer

Superlattice wafers (IQE Ltd., Cardiff, U.K.) of alternating layers of GaAs/$Al_xGa_{(1-x)}$As were cleaved into small pieces, and GaAs selectively etched away in NH_4OH:H_2O_2:H_2O (1:20:300 v/v) to expose a comb of parallel AlGaAs ridges running along the cleaved edge. 100 Å of Pt was evaporated at a 45° angle to coat just the tips of the ridges, forming an array of parallel Pt nanowires running along the edge. The superlattice chip was then placed array-side down onto the doped SOI substrate with a home-built aligner system (Figure 1c), and held in place by a thin layer of thermally-cured epoxy that had been previously spun onto the substrate. After curing, the entire assembly was placed gently in a H_2O_2:H_3PO_4:H_2O (1:5:50 v/v) solution to dissolve the GaAs/AlGaAs superlattice chip, leaving the array of Pt nanowires immobilized on the substrate (Figure 1d).

Contact metallization

The chips were dipped into BOE:H_2O (1:25 v/v, 10 s in dark) to remove oxides over the contact regions before Ti/Pt/Au (100/100/1200 Å) contacts were evaporated onto the devices (Figure 1d).

Irradiance and wavelength calibrations

Our illumination system consists of an Oriel 150 W Xe arc lamp source coupled at *f*/4 through a home-built cut-on filter changer to an Oriel MS257 monochromator (Newport Corp., Stratford, CT). The divergent output from the monochromator was collimated into a ~1 cm diameter spot at the sample plane using a plano-convex f = 75 mm lens (Thorlabs Inc., Newton, NJ). We selected "UV-grade" fused silica for all optical elements to maximize transmission of the ultraviolet wavelengths.

The irradiance calibration reference is a Hamamatsu S1337-1010BQ silicon photodiode (Hamamatsu Corp., Bridgewater, NJ), calibrated between 250-1100 nm to NIST-traceable standards (Opto-Cal Inc., Lakeside, CA) and mounted behind a 500 μm

diameter precision pinhole (Edmund Optics, Barrington, NJ). The wavelength-dependent irradiance was measured in the center of the collimated beam at the sample plane using a 10 nm bandpass in steps of 1 nm. We have also measured the irradiance spectrum with an uncoated Glan-Thompson linear polarizer (Thorlabs Inc., Newton, NJ) mounted just before the detector and find that there is only a slight polarization introduced by the illumination system.

Wavelength calibrations were regularly performed, often before each set of measurements, using the sharp emission lines from a Hg(Ar) pen-style lamp (Newport Corp., Stratford, CT) at the input of the monochromator and the reference photodiode at the sample plane. For each of the gratings used, the monochromator was scanned in 0.1 nm steps in the vicinity of a strong emission line. The position of the peak was used to calibrate the monochromator wavelength readout, and was typically reproducible to ~0.1 nm. At the end of each wavelength calibration, monochromator slit functions were also measured at 10 nm bandpass in steps of 0.1 nm to characterize the instrumental broadening of the illumination system. The slit functions were nearly perfectly triangular and identically wide for all gratings used, indicative of a well-aligned optical system.

Rigorous coupled-wave analysis calculation

The rigorous coupled-wave analysis (RCWA) represents periodic surface features as a Fourier series and propagates the incident wave through the optical model by solving Maxwell's equations exactly. Essentially, a three-dimensional grid is overlaid over a unit cell of the periodic structure, and the optical model is built up layer-by-layer by assigning appropriate optical constants to each volume element. In each layer, the periodic pattern of optical constants is assumed to be constant throughout the entire layer thickness and is approximated as a truncated Fourier series. The illumination conditions are then defined and the differential equations solved layer-by-layer as the incident wave enters the structure from the superstrate and exits via the substrate. Special care is taken to match the electromagnetic boundary conditions at each interface. In this way, the reflected and transmitted diffraction amplitudes are obtained for the entire multilayer structure, from which the reflectance and transmittance can be calculated for any given diffracted order. The reflectance is evaluated at the upper interface between the superstrate and the topmost layer, while the transmittance is evaluated at the lower interface between the bottommost layer and the substrate.

There is no general restriction on the grid resolution, uniformity or geometry, so we have used a somewhat coarse (1 nm × 1 nm) uniform square grid to discretize the nanowire array for speed and simplicity. The superstrate (air or vacuum) and substrate (680 μm thick silicon handle wafer) media are assumed to be continuous, isotropic and infinite. For a grating structure like our nanowire arrays with features dependent on the x,y,z-space coordinates, the Fourier series is one-dimensional in x (normal to the nanowires). In the y-direction (parallel to the nanowire axis) the features are assumed to be infinite in extent, which is a reasonable approximation given that our arrays are ≥10 μm long, more than 10 times longer than the wavelengths of interest. In the z-direction, we used 3 layers to represent the bulk film device (see Figure 2a) and 17 layers to represent the nanowire array structure (Figure 2b). A total of 65 Fourier modes were included in the calculation assuming normal incidence plane-wave illumination. To calculate the absorptance $A = 1 - R - T - S$, we used the zero-order (specular) reflectance

R_0 and transmittance T_0 and assume no scattering (S = 0). We have verified that the reflectance and transmittance are identically zero for non-zero diffraction orders; this implies complete absorption and therefore evanescent diffracted waves for higher orders.

Diode and photovoltaic characterization

A few sets of thin film and NWA devices were fabricated. The devices described in the main text were chosen for optical characterization because they appeared, by light microscopy inspection, to be the most homogeneous. The devices chosen were selected for the absence of irregularities due to fabrication variability, so as to avoid artifacts in the measured optical data. Dark I-V curves were also obtained for those (and other) devices with a Model 6430 sourcemeter (Keithley Instruments, Cleveland, OH) by sourcing voltage and measuring current.

Figure 2 in the main text shows clear diode responses from a set of devices with high-dose doping (3.8×10^{13} cm^{-2} B$^+$) in the device regions. These higher-doped nanowire array devices generate I_{sc} = 17 pA and V_{oc} = 0.26 V with FF = 0.50, while the higher-doped film devices develop I_{sc} = 28 pA and V_{oc} = 0.37 V with FF = 0.62. However, the higher-doped nanowire arrays were of poorer structural quality and were less amenable to optical modeling. Hence we have chosen to focus on the lower-doped (3.8×10^{10} cm^{-2} B$^+$) principal device in the main text.

In Table S1 we summarize additional measurements from other devices. We note that the nanowire array devices tend to exhibit more scatter in their properties, while the film devices are essentially homogeneous. The photovoltaic properties do not exhibit any dependence on device length as the minority carrier diffusion lengths are far smaller than the geometrical dimensions of the device. On the whole, our devices are comparable in performance to previously reported examples of silicon nanowire photovoltaics in the literature.

Minority carrier diffusion length

Minority carrier diffusion lengths were measured using a WITec AlphaSNOM (WITec Wissenschaftliche Instrumente und Technologie GmbH, Ulm, Germany) scanning near-field optical microscope (SNOM). Light from laser diodes at 405 nm (blue) or 650 nm (red) was chopped at 83 Hz and fiber-coupled into the microscope. An objective lens was used to focus the laser light onto the device (far-field illumination), or onto the 100 nm aperture of a SNOM tip (near-field illumination). The device was mounted on a computer controlled stage under the objective lens, connected to a SR570 current-to-voltage preamplifier and the preamplifier output voltage measured with a SR830 lock-in amplifier (Stanford Research Systems Inc., Sunnyvale, CA). To acquire the scanning photocurrent images, the laser probe beam was rastered across the device while recording the lock-in output as a function of probe position. During the measurement, the devices were weakly illuminated using the microscope lamp to remove artifacts arising from light absorption in the substrate wafer. The minimum illumination level was used to remove capacitance transients from the output photocurrent so as to obtain a square wave output.

Scanning photocurrent images acquired with far-field illumination were resolution-limited by the quality of the focusing objective or by focusing errors (Figure S1). On the other hand, near-field illumination using the SNOM tip in contact-mode

enabled high-resolution measurements of the diffusion length limited only by the tip aperture size (Figure S2). Unfortunately, because the tip is dragged across the surface, the sample undergoes damage during the measurement and can typically only tolerate a few repeat measurements. After the measurement, line profiles were taken along the device axis and fitted to an exponential function to determine the diffusion lengths on either side of the junction.

Cross-sectional transmission electron microscopy

Focused-ion beam (FIB) liftout of the cross-sectional sample was performed in a Nova 600 DualBeam FIB/SEM (FEI Company, Hillsboro, OR) equipped with an Autoprobe 200 micromanipulator system (Omniprobe Inc., Dallas, TX). Initial cuts were made at a higher ion energy of 30 kV and high beam currents of >1000 pA for increased speed. Final thinning to electron transparency was performed with ions at 10 kV at glancing incidence and lower beam currents of <100 pA to minimize sample damage.

After the cross-section was prepared, it was loaded into a Tecnai TF20ST TEM (FEI Company, Hillsboro, OR) for imaging at 200 kV. Sometimes, the cross-sectional sample was too thick, and contained contrast contributions from inelastically scattered transmitted electrons. In that case, a Gatan Imaging Filter (Gatan Inc., Pleasanton, CA) was used to image the zero-loss electrons and provided improved contrast (Figure 3a,b in main text). Convergent beam electron diffraction (CBED) was performed by focusing the beam to crossover over the device regions and capturing the diffraction patterns on a charge-coupled device at the camera plane (Figure S3a,b). With sufficiently thin sample regions, high-resolution transmission electron micrographs were acquired along the [011] zone of the sample and confirm that the high crystallinity of the devices are retained after processing (Figure S3c). By placing an objective aperture about the $(\bar{1}11)$ spot, tilted-beam dark-field micrographs also show that the devices remain crystalline (Figure S3d).

Table S1. Measured parameters of some of our devices, compared to literature reported values for silicon nanowire photovoltaic devices. Where possible, we have calculated the short-circuit current density J_{sc} using the projected active area $Y = L \times W$ of the device. Ideality factors n_{lit} and n_{dark} were obtained by fitting lit and dark I-V measurements to the diode equation $I = I_0 [\exp(qV/nk_BT) - 1]$ in the low forward bias region (up to ~0.4 V).

Sample	I_{sc} (pA)	J_{sc} (mA/cm^2)	V_{oc} (V)	FF	n_{lit}	n_{dark}	Description
3.8×10^{13} cm^{-2} B^+ dose							
NWA	17		0.26	0.50	2.2	2.7	10 μm long
NWA	17		0.34	0.60	1.8	1.8	10 μm long
NWA	17		0.34	0.55	2.2	1.9	25 μm long
Thin Film	28		0.37	0.62	1.5	1.9	10 μm long
Thin Film	27		0.36	0.60	1.6	1.8	10 μm long
Thin Film	27		0.37	0.62	1.8	1.7	25 μm long
NWA	18		0.26				25 μm long
NWA	19		0.38				50 μm long
NWA	19		0.35				100 μm long
Thin Film	29		0.40				25 μm long
Thin Film	30		0.40				25 μm long
Thin Film	29		0.39				100 μm long
3.8×10^{10} cm^{-2} B^+ dose							
NWA[a]	26	2.6	0.37				10 μm long
Film[b]	60	3.0	0.46				10 μm long
Literature values							
Ref. 3		5.0	0.19	0.40		3.6	Axial Schottky
Ref. 4	3.5		0.12		1.78		Axial p-n
Ref. 4	14.0		0.24				Axial p-i-n, i=2 μm
Ref. 4	31.1	3.5	0.29	0.51	1.28		Axial p-i-n, i=4 μm
Ref. 5		4.28	0.29	0.33		2.1	Radial p-n
Ref. 2	503	23.9	0.26	0.55	1.86	1.96	Radial p-i-n

a) This device corresponds to the array device in Figures 3 and 4.
b) This device corresponds to the film device in Figures 3 and 4.

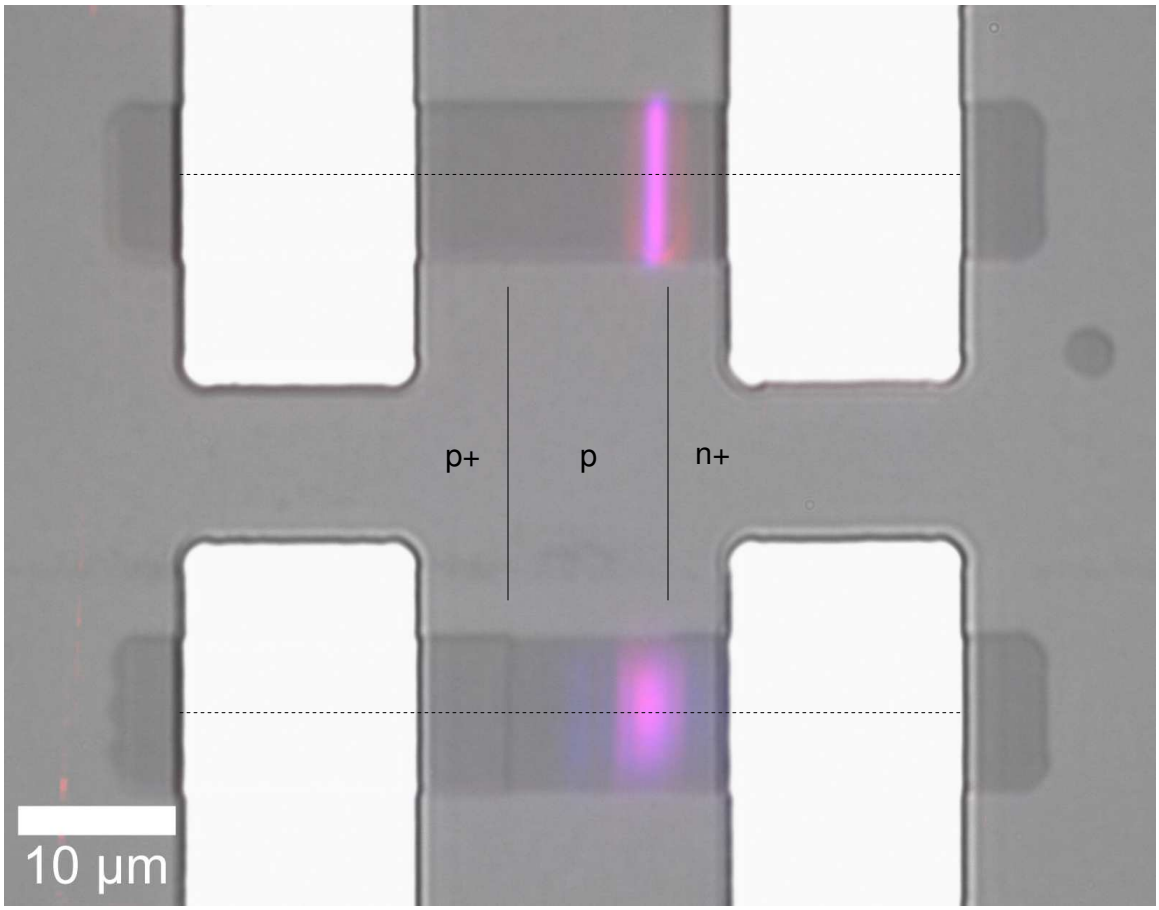

Figure S1. Optical micrograph of bulk film (top) and nanowire array (bottom) devices, overlaid with far-field scanning photocurrent images obtained at 405 nm (blue) and 650 nm (red). The excellent overlap between the red and blue photocurrent images (purple) indicates that there is no wavelength dependence for the minority carrier diffusion length. There is some spurious intensity in both blue and red photocurrent images even in regions far away from the junction due to beam reflections and a poorly focused probe beam.

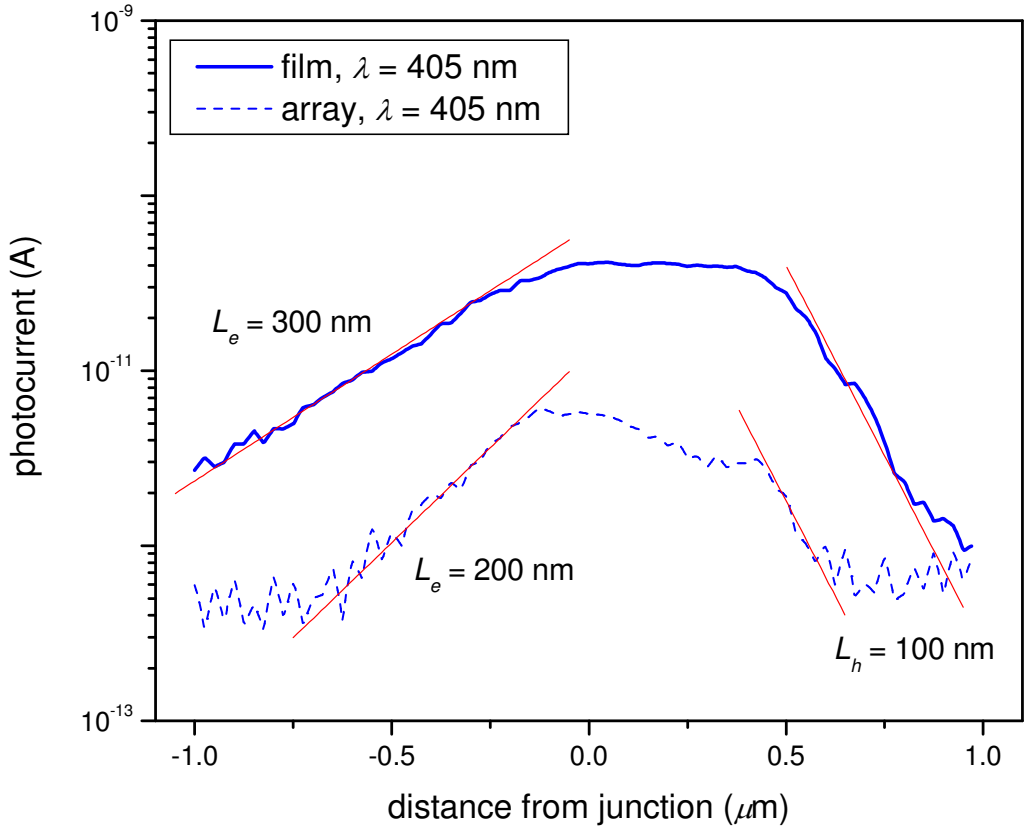

Figure S2. Line profiles through near-field scanning photocurrent images obtained with a scanning near-field optical microscope (SNOM) in contact mode, taken along the dashed lines in Figure S1. An exponential fit on the left (right) side of the peak yields the minority carrier diffusion length L_e (L_h), with measurement resolution determined by the finite size of the SNOM tip aperture (100 nm). This yields upper estimates for the total diffusion length L_{max} ~ 400 nm and 300 nm respectively for the bulk film and nanowire array devices. Accounting for the broadening due to the tip aperture, the respective lower estimates are L_{min} ~ 200 nm and 100 nm.

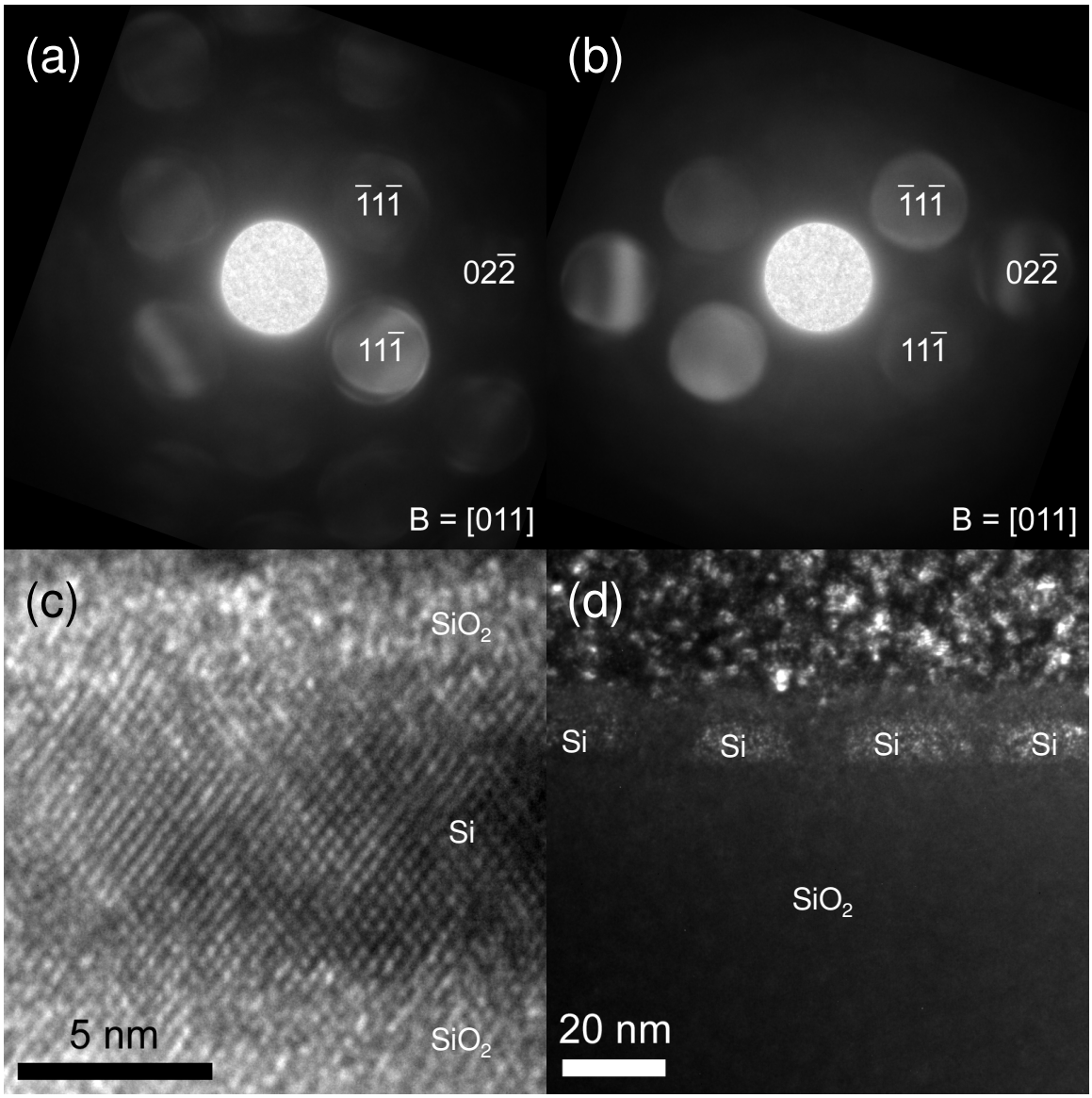

Figure S3. Convergent beam electron diffraction (CBED) patterns of (a) bulk film and (b) nanowire devices, taken along the B = [011] zone (parallel to the nanowire axis). As expected, the CBED patterns are identical since both devices are fabricated from the same starting substrate. (c) Cross-sectional transmission electron microscope (XTEM) image of bulk film device down B = [011], showing high crystallinity of the film. (d) Tilted-beam dark-field XTEM image of the nanowire array device formed with the (111) spot. All nanowires within the field are crystalline.